Soft Matter

Fabricating Mesoscale Polymer Ribbons with Tunable Mechanical Properties via Evaporative Deposition and Dewetting

Journal:	*Soft Matter*
Manuscript ID	SM-ART-03-2024-000368.R1
Article Type:	Paper
Date Submitted by the Author:	17-May-2024
Complete List of Authors:	Meissner, Cornelia; University of Massachusetts Amherst, Polymer Science and Engineering Bhamla, M.; Stanford University, Chemical Engineering Emrick, Todd; University of Massachusetts Amherst, Polymer Science and Engineering Crosby, Alfred; University of Massachusetts, Polymer Science and Engineering

ARTICLE

Fabricating Mesoscale Polymer Ribbons with Tunable Mechanical Properties via Evaporative Deposition and Dewetting

Cornelia Meissner, M. Saad Bhamla, Todd Emrick* and Alfred J. Crosby*

Received 00th January 20xx,
Accepted 00th January 20xx

DOI: 10.1039/x0xx00000x

Synthetic replication of the precise mesoscale control found in natural systems poses substantial experimental challenges due to the need for manipulation across multiple length scales (from nano- to millimeter).We address this challenge by using a 'flow coating' method to fabricate polymer ribbons with precisely tunable dimensions and mechanical properties. Overcoming barriers that previously limited the achievable range of properties with this method, we eliminate the need for substrate patterning and post-processing etching to facilitate the production of high aspect ratio, filament-like ribbons across a range of polymers—from glassy polystyrene to elastomeric poly(butadiene), as well as block poly(butadiene-block-styrene). Our method uniquely enables the preservation of chemical fidelity, composition, and dimensions of these ribbons, leveraging polymers with elastic moduli from GPa to tens of MPa to achieve multi-scale features. We demonstrate the role of the elastocapillary length (γ/E) in determining morphological outcomes, revealing the increase in curvature with lower elastic modulus. This finding underscores the intricate relationship between surface tension, elastic modulus, and resultant structural form, enabling control over the morphology of mesoscale ribbons. The soft (MPa) polybutadiene-based ribbons exemplify our method's utility, offering structures with significant extensibility, resilience, and ease of handling, thus expanding the potential for future applications. This work advances our understanding of the fundamental principles governing mesoscale structure formation and unlocks new possibilities for designing soft materials with tailored properties, mirroring the complexity and functionality observed in nature.

Introduction

Amidst ongoing progress in soft materials at the macro- and nanoscale, numerous opportunities are presented by mesoscale materials (Figure 1), where elasticity, interfacial forces, and geometry work collectively and cooperatively. Mesoscale engineering is ubiquitous in nature and is responsible for generating a breadth of physical and mechanical properties from a basic set of building blocks. For example, tendon and skin are composed of collagen fibrils, but the elastic modulus of tendon is two orders of magnitude greater than that of skin. This difference arises from the ordered mesoscale structure associated with tendon, with aligned collagen fibrils[1] that contrasts their amorphous characteristics in skin (Figure 1).[2] Dimensional variation and alignment in collagen microfibrils also impact biomechanics, seen for example in joint hypermobility in mice when expression of one type of collagen protein is deleted in tendons and ligaments.[3] Understanding the fundamental impacts of mesoscale structure stands to enhance human health, as the effects resulting from joint hypermobility range from modest to severe.[4] In plants, the cellulose microfibrils that form tendrils dictate macroscale helicity, such as in the squash tendril where helicity is induced by the intracellular cellulose microfibrils.[5] Individual (isolated) straight mesoscale structures are likewise prevalent in nature, such as bacteria flagella, with moduli on the order of MPa, that drive underwater motion.[6] The California blackworm, a high aspect ratio animal, aggregates into floating buoys that respond to external stimuli, such as oxygenation levels, producing assemblies akin to fluids of varying viscosity.[7] These and other examples from nature inspire syntheses of soft mesoscale objects, where the expansive sets of properties available from soft materials offer tremendous flexibility in materials designs and interactions.

As efforts to organize mesoscale materials grow in recent years,[8,9] such structures are often limited to stiff materials and energy-intensive syntheses, such as to achieve rigid pillars[10–12] or complex polyhedra.[13] Evaporative deposition has been used to realize flexible structures ranging from thin films to grids and filaments of different geometries from stiff materials like gold nanoparticles, quantum dots and glassy polymers.[14–16] Soft materials with a modulus in the range of MPa have not been deposited prior to this work. Detailed knowledge of mesoscale structures will propel engineering of new soft materials on size scales that are challenging to access synthetically.

Our mesoscale engineering approach to producing filamentous soft materials utilizes an evaporative deposition method, termed 'flow coating'[15], yielding flat structures of ~ 20 µm width, ~700 nm thickness, and cm in length. Experimentally,

Polymer Science and Engineering Department, University of Massachusetts Amherst, Conte Center for Polymer Research, 120 Governors Drive, Amherst, MA 01003

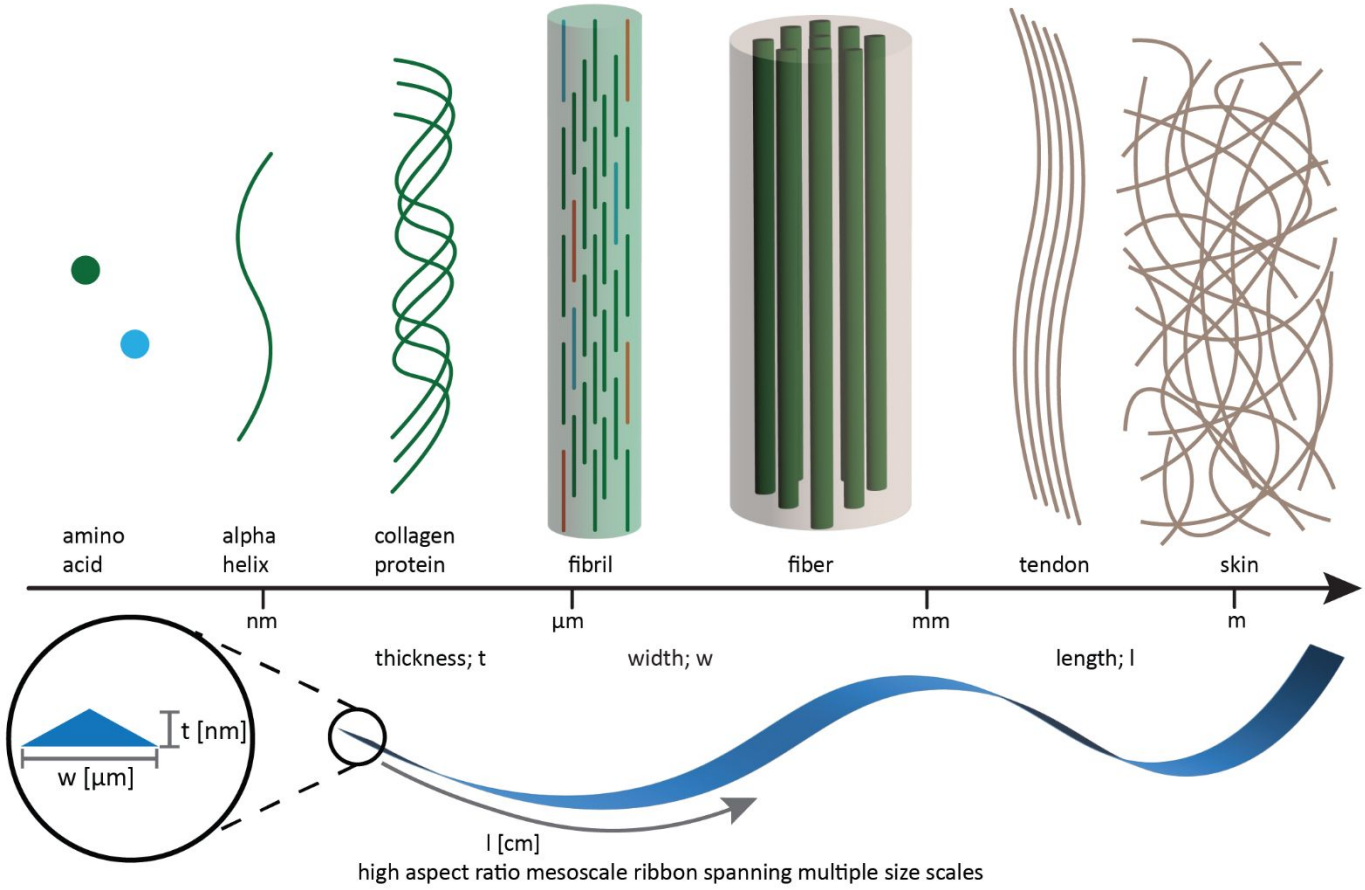

Fig. 1 Top: Hierarchical biomaterials assembly over several orders-of-magnitude length scales generates a library of materials properties from a subset of naturally occurring chemical building blocks. Bottom: Synthetic mesoscale ribbons span several size scales with nm thickness, µm width, and mm length.

the process utilizes a substrate supported on a programmed, translating stage that directs solute deposition to the edge of a blade, which is held with micromanipulators at a ~30° angle and ~200 µm above the substrate (see SI for detailed description and photograph (Figure S1)). To prepare the ribbons, a few microliters of a dilute polymer solution (3 mg/mL) in toluene are added by micropipette to the area of the substrate in front of the blade. Capillary forces wick the solution under the blade, such that the contact line mimics the contour of the blade, and the stage is translated at ~3 mm/sec.[17] Intermittently, the motion is paused (the dwell time), whereupon solvent evaporation yields ribbon formation at the contact line, a process that uses evaporation-driven flows resembling the classically studied 'coffee ring effect'.[18] The surface roughness resulting from deposition favors pinning or sticking of the contact line, until translation of the substrate relative to the blade breaks the capillary bridge after the minimum receding contact angle has been surpassed. The contact line moves across the substrate and stops at prescribed locations to deposit the next ribbon. The resultant polymer ribbons are multi-length scale structures (10^{-2} m length, 10^{-5} m width, and 10^{-7} m maximum thickness) with a triangular cross-section (see Figure 1, Figure S4, and Figure S5). As previously shown, when released from the substrate into a fluid, the unique geometries of these filamentous structures induce helix formation for thin, soft materials, which may be understood according to Eq 1:

$$R = \frac{Et^2}{12\gamma}\left(\sqrt{\frac{1}{4}+\left(\frac{t}{w}\right)^2}-1\right)^{-1} \quad \text{Eq 1}$$

where R is the radius of curvature of the helix, E is the elastic modulus, γ is the interfacial tension, t is the ribbon thickness, and w is the ribbon width.[19]

Prior to this work, polymer-based ribbon preparations using flow coating techniques required an etching step, such as reactive ion etching or oxygen plasma treatment, to remove a thin polymer film that inter-connects the individual mesostructures.[19,20] Such treatment proves effective at generating individual ribbons but may alter the surface chemistry and geometry of the ribbons, due to the necessary exposure of the entire system (*i.e.*, both ribbons and inter-ribbon film) to the etchant. Rather than removing the inter-ribbon layer, a more efficient approach would prevent its formation at the outset, which in principle may be accomplished by spatially tuning substrate wettability (surface energy). For example, patterning of the substrate has been employed to initiate dewetting of polymer solutions in pre-determined areas,[21] which in turn dictates the deposition of subsequent layers. However, such methods are laborious and lack flexibility concerning the dimensions and shapes of the deposited materials. In our work, we find that certain polymers allow for the deposition of polymer ribbons without a connecting film, thus precluding the need for subsequent

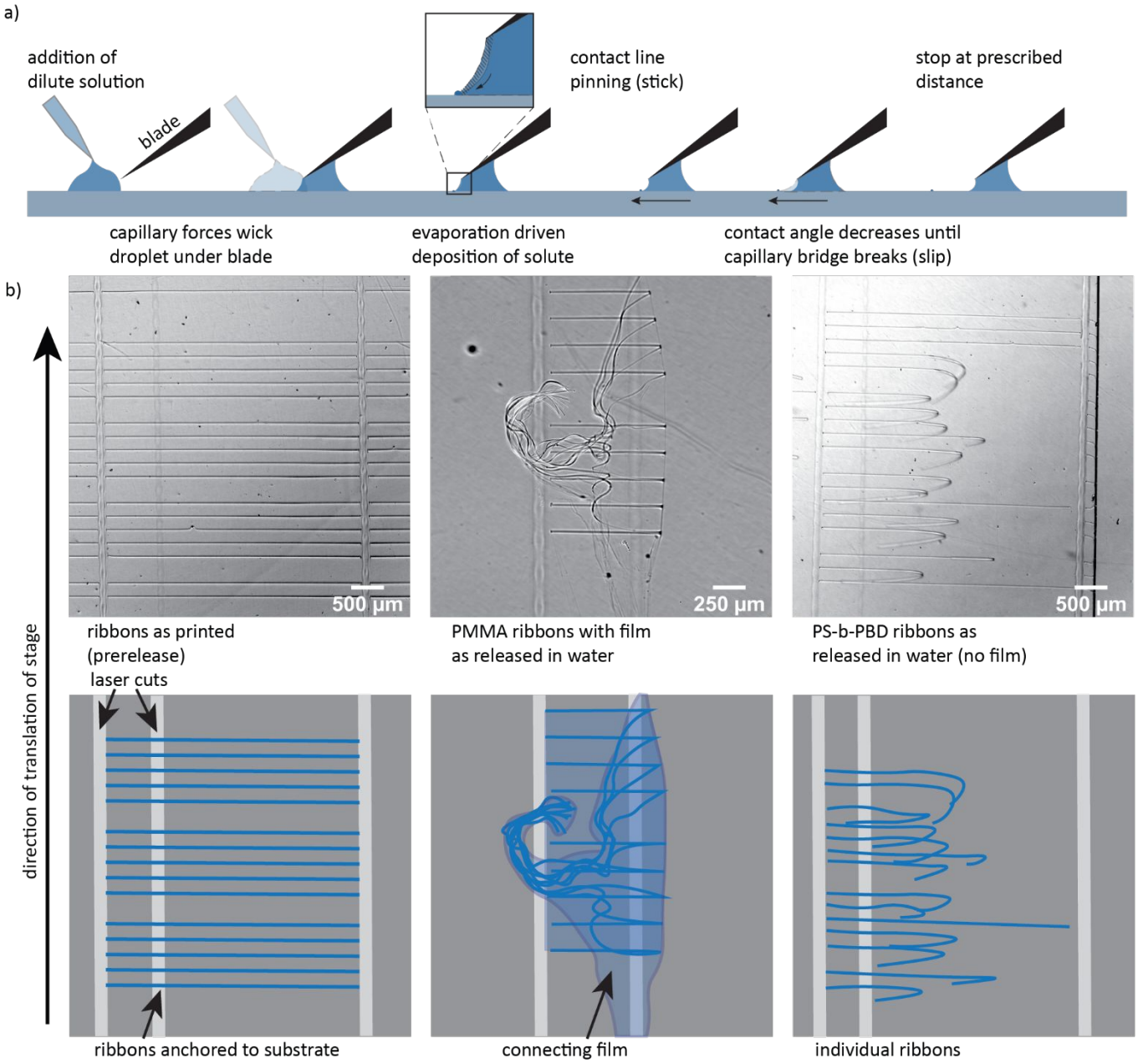

Fig. 2 (a) Schematic description of the flow coating process and (b) optical micrographs and schematics of resulting ribbons after laser cutting steps. Schematic shows blue ribbons, and light gray laser cuts (one anchoring cut before deposition and one size-determining cut after deposition) on a dark gray substrate. PMMA ribbons released in water are connected by an inter-ribbon film (see also movie S1). PS-b-PBD (88.5kDa-b-90kDa) ribbons released in water have no connecting film.

etching steps, which we could explore while tuning elastic modulus. Specifically, flow coating of polystyrene (PS) and polybutadiene (PBD)-based block polymers leads to the deposition of distinct ribbons, conforming to the shape of the blade edge, without prior substrate patterning. Solutions of PS-*b*-PBD block copolymers were found to dewet the substrate at a critical thickness that is below the ribbon thickness, allowing ribbon deposition at mesoscale dimensions and with high fidelity. As will be described, polymer/fluid/substrate/air interfacial interactions influence the outcome of these experiments, with some polymer compositions generating inter-ribbon films (poly(methyl methacrylate) (PMMA)), and others dewetting completely (PS-random-PBD). Interestingly, flow coating deposition methods using PS and PS-block-PBD give access to mesoscale ribbons of vastly different elastic moduli and tuning the PS:PBD ratio in block polymer structures yields morphologies ranging from straight (glassy) to helical (rubbery) in fluid media.

Results and Discussion

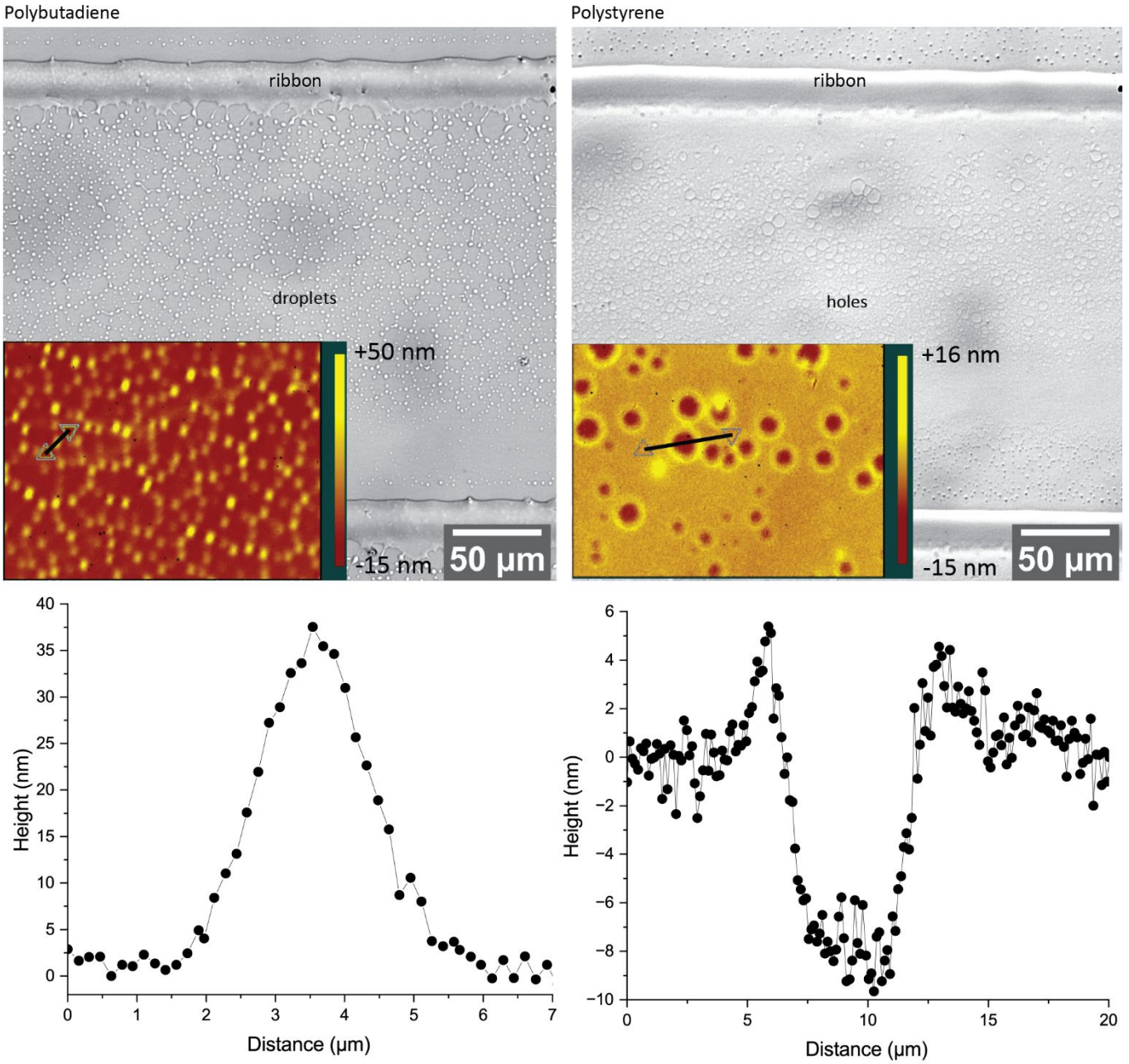

Fig. 3 Optical micrographs of polybutadiene showing droplet formation and of polystyrene showing the hole formation across the inter-ribbon area. The ribbons are printed horizontally across at the top and bottom of the optical micrograph with an inter ribbon distance of 250 µm where dewetting is observed. Inset: surface maps of the inter-ribbon area of polybutadiene and polystyrene, lines indicating the position at which data was taken for the height trace shown below. Height traces indicating droplet of 40 nm height and 5 µm width for the PBD sample and a hole of 10 nm depth with 6 nm rim and 10 µm width for the PS sample.

The flow coating experiments described in this study employed commercial samples of PS (143 kDa), PS-b-PBD (PS(26.8 kDa)-b-PBD(70 kDa), PS(88.5 kDa)-b-(90 kDa), PS(35 kDa)-b-PBD(11 kDa), PS(75 kDa)-b-(3 kDa)), and PBD (163 kDa), as well as poly(methyl methacrylate) (PMMA, 243 kDa) as a comparative polymer that has been used in prior reports on flow coating (full experimental details provided in the SI).[16,19,20,22] Flow coating was performed on clean glass slides that had been coated with a ~50 nm film of poly(styrene sulfonate) (PSS), which functions as a release layer. Portions of the PSS layer were removed with an infrared laser to expose lines of bare glass at ~4 mm intervals – these serve as anchor points for the deposited ribbons. Orthogonal to the anchoring regions, PMMA ribbons were deposited following the direction of the blade edge, by flow-coating from a 3 mg/mL toluene solution (compare Figure 2a)). The stage was translated at 3 mm/s for 250 µm, with a dwell (stopping) time of 8 s, yielding structures of ~24 mm length which were then laser-cut into 4 mm pieces. The second iteration of laser-cut lines follows in proximity and parallel to the first set of lines. As illustrated in Figure 2, this anchors one end of the ribbons to the glass slide while the unanchored portions of the ribbon can disperse in the fluid phase. Submersion of the flow-coated substrates into aqueous media dissolves the hydrophilic PSS layer to reveal a set of ribbons that are inter-connected by a thin film of PMMA that folds over with the ribbons (shown as blue in the

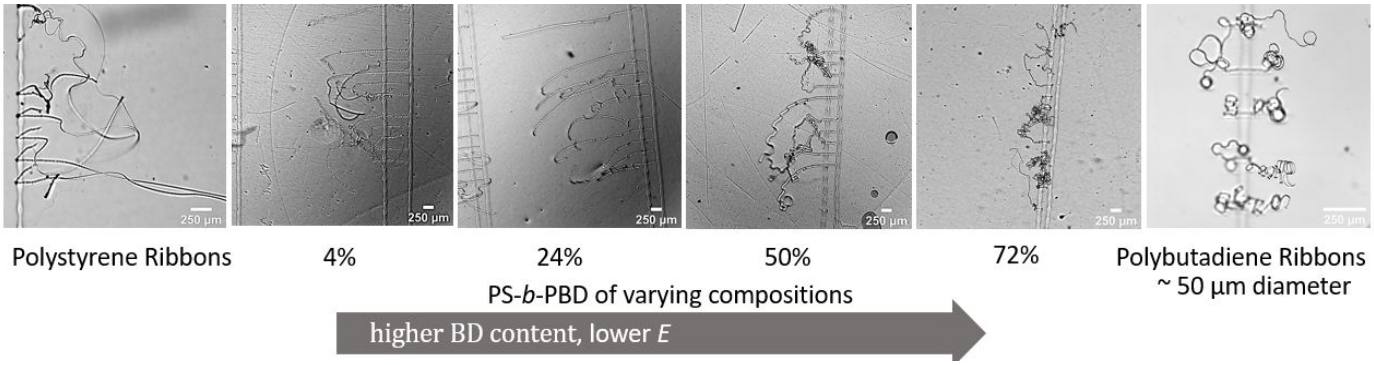

Fig. 4 Optical micrographs of PS, PBD, and the block polymers of varying PBD content. As f(BD) increases, the elastic modulus decreases, resulting in higher curvature of their steady state morphologies.

accompanying schematic). By optical microscopy, one sees the vertical line of the laser cut at which the ribbons are attached to the glass slide as well as the second laser cut that releases the ends (light grey in the schematic). Note that in the optical micrograph, the edge of the film, where the ribbons fold back, appears distinctly darker. When in the aqueous phase, the ribbons coil in parallel and are directed towards one other, in a motion that is restricted by the connecting film. This ribbon-reinforced thin film collapses at the free end. When the microscope stage is moved, the ribbons move in parallel, with the maximum inter-ribbon distance determined by the original deposition (see Movie S1 for inter-connected PMMA ribbons in motion).

Similar flow-coating experiments were then performed with PS and PS-b-PBD block polymer (50:50 ratio) while maintaining similar experimental parameters (solvent, solution concentrations, sacrificial layer preparation, dwell time, translation speed, and blade height). Under these conditions, the resulting polymer ribbon had dimensions comparable to that of the PMMA ribbons, but with a notable absence of any appreciable inter-ribbon layer following their preparation. Thus, as seen in Figure 2, removal of the sacrificial PSS layer by dissolution in water to release the polymer ribbons resulted in discrete mesoscale structures unimpeded by any connecting film which in turn gives the structures greater degrees of freedom presenting as individual morphologies and movement when visualized by optical microscopy.

The dependence of film (or “scum layer”) formation on polymer composition arises from the simultaneous and competing roles of polymer sedimentation, adsorption, and evaporation-driven deposition as the contact line traverses the substrate between dwell times and ribbon deposition. Thus, the difference in scum layer formation depends on the propensity of a given polymer to deposit on the substrate (irrespective of the mechanism) between ribbon formation (i.e., where evaporative deposition dominates) with the results above showing significant differences between PMMA and the PS and PBD-containing polymers. Optical microscopy and profilometry measurements shown in Figure 3 allow for an in-depth probing of the inter-ribbon area. For example, optical microscopy of a flow coated PBD sample showed lighter features between ribbons (running from left to right at the top and bottom of the image) (Figure 3). These lighter dots spread from one ribbon to the next and are arranged along lines (polygon shape) indicating that they were formed via a dewetting process that started from a thin film which formed holes that widened until the rims formed lines that then resulted in the observed white droplets.[23,24] Optical profilometry provides the necessary height data to confirm these features to correspond to droplets. We chose one of the droplets in the 2D optical profilometry graph showing the topological features with lighter colors corresponding to higher regions, to demonstrate height and width. As shown in the height trace (Figure 3) the droplets reach a height of tens of nanometers and a diameter of several micrometers.

The optical micrograph of the polystyrene sample shows dark circles in the inter-ribbon area (Figure 3), corresponding to the thicker rims surrounding holes grown in the thin PS inter-ribbon layer. The surface map acquired by optical profilometry (Figure 3) shows the height map of some inter-ribbon film. The darker circles correspond to the holes in the film (PS). The bigger holes have a diameter of about 10 µm. Holes in a thin film that result from dewetting grow in depth, then in width, typically reaching the substrate.[23] The hole depth in the PS film is ~10 nm, with a 6 nm rim around the hole. This indicates an initial PS film thickness of 10 nm between ribbons.

Previous research on polymer thin film dewetting, which has been studied extensively,[25–28] shows that the holes in polystyrene thin films often form as a result of heterogeneous nucleation from defects. These holes then widen to form a network of connected polygonal patterns composed of polystyrene that reduce the area of the interface by forming droplets on the corners of the polygons, absorbing the connecting lines.[23] This process is faster at higher temperatures and in thinner films.[23,24,29,30] In our polymer system, the higher fraction of PBD translates to higher mobility (comparable to higher temperatures for the same polymer) displaying dewetting behavior further along in this process. Pure polystyrene film shows hole formation and even the addition of just 4% PBD (see Figure S2 F) as part of the block polymer results in notably more holes than the PS homopolymer and first droplets about 125 µm from the initial ribbon. The 50:50 polymer (Figure S2 D) shows dewetting similar to spinodal dewetting.[31] This trend continues for the pure poly(butadiene), which forms droplets on the substrate between the two ribbons

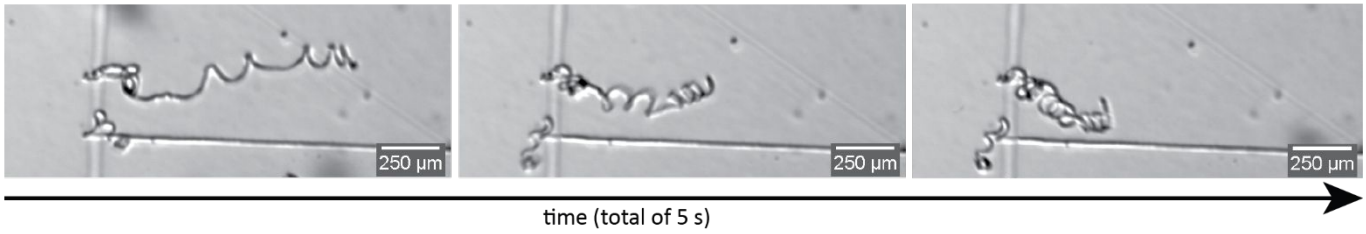

Fig 5. Time sequence of a single polybutadiene ribbon coiling taking a total time of 5 s. Separate snapshots show the formation of new coils taken from movie S2.

(Figure 3, Fig S2 B). Notably the PMMA film (A) does not display any dewetting behavior, explaining the observed films after release. In our experiments, both homopolymer PS and PBD and their respective block polymers left no connecting film while successfully forming stable ribbons. To determine whether this dewetting behavior was purely dependent on the composition of the PS/PBD polymer or dependent on the molecular block architecture, we flow-coated ribbons from a random copolymer PS-r-PBD (304 kDa, PS 45 mol%). The random copolymer appears to aggregate in droplets on the PSS surface, forming no connected ribbons and falling apart upon release.

We deposited ribbons of similar dimensions (600-900 nm height, 20-25 µm width) from the various block polymers and released the ribbons in RO water to observe their morphology: each formed distinct ribbons, demonstrating the ubiquity of the dewetting behavior (see Figure 4). The released PS-b-PBD ribbons show a trend of increasing curvature from linear to helical coils as the fraction of PBD increases (Figure 4). The difference in morphology can be explained by the previously introduced scaling (Eq 1). As the elastic modulus of the starting material decreases by several orders of magnitude (PS ~ GPa to PBD ~ MPa) the elastocapillary length, defined as the ratio of surface tension to elastic modulus, γ/E, approaches the ribbon thickness and induces a higher curvature. Previously, Pham, *et al.* showed that ribbons made of glassy PMMA polymer, gold nanoparticles, or quantum dots, can form helical coils as the thickness of the ribbon approaches the elastocapillary length.[19]

Here we show that this scaling can describe the morphology of ribbons of comparable thickness with varying elastic moduli. While the PBD-based ribbons form helices, the PS ribbons do not form helices on these length scales, due to the interplay of interfacial tension and elasticity.

The resulting radius of the PBD helices can be estimated from the microscopy images to be 26 ± 4 µm (details in the SI). Using this radius and equation 1 we can estimate the elastic modulus E of PBD. We take the interfacial tension from literature[32] 43.1 mJ/m^2, the thickness of the ribbons 921 ±7 nm from optical profilometry measurements prerelease as well as the t/w aspect ratio of the sample 0.04 ± 0.01 to estimate an elastic modulus of 32 MPa (a more detailed description of our measurements and statistics are provided in the SI). This modulus is slightly greater than the 4 MPa / 1.6 MPa elastic moduli that can be calculated from the shear moduli found in literature for similar PBD in air, assuming a Poisson's ratio of 0.5.[33,34] This discrepancy may be attributed to the differences in the processing conditions as well as the thin nature of our ribbons, which may dimensionally confine[35,36] the polymer molecules for our materials, as compared those values reported in literature.

In Figure 5, a sequence of five images describes the path of helical coiling of a single PBD ribbon. The ribbon starts out in a lengthened position then, when the slide is exposed to water, the sacrificial layer of PSS dissolves and coiling begins. This first image of the sequence shows a stretched ribbon measuring over 1 mm in total length (the distance between laser cuts is 4 mm, describing the contour length of the helix); over time, the axial helix length shortens via two mechanisms. The number of coils increases, as seen in the first three frames of the sequence. Subsequently and in parallel, the pitch (i.e., the distance between helical coils) decreases and a tighter helix forms. The final product is a helix with coils of similar radius (~25 µm), prescribed by the ribbon material, geometry, and the surrounding aqueous solution as described in Eq 1. The full sequence can be seen in Movie S2.

Conclusions

Evaporative deposition (flow coating) is a facile method to generate mesoscale polymer structures using a solution deposition process that requires no pre-patterning or post-etching steps. The process exploits wettability of the substrate and inherent surface tension and mobility of the deposited polymers. The mesoscale ribbon-like structures may be composed of a variety of polymer types, including glassy polystyrene, elastomeric poly(butadiene), or block poly(butadiene-block-styrene). The methods described yield high aspect-ratio filamentous structures using polymers with moduli values spanning several orders of magnitude, from GPa (polystyrene) to MPa (polybutadiene). These bulk properties translate to the mesoscale ribbons with their solution morphologies, from straight to helical, as the polymers become softer. Inherent dewetting behavior can be exploited for deposition of discrete mesoscale structures, opening possibilities for future functionalization, as well as extreme softness and stretchability relative to other synthetic mesoscale structures.

Author Contributions

C.M.: conceptualization, data curation, formal analysis, investigation, project administration, visualization, writing – original draft. M.S.B.: writing – review & editing. T.E. & A.J.C.: funding

acquisition, project administration, resources, supervision, writing – review & editing.

Conflicts of interest

There are no conflicts to declare.

Acknowledgements

This work was supported by the National Science Foundation (NSF EAGER, No. 2218119) and the Human Frontier Science Program (HFSP, No. RGP0019/2017).

References

1 M. A. Meyers, P.-Y. Chen, A. Y.-M. Lin and Y. Seki, *Progress in Materials Science*, 2008, **53**, 1–206.

2 A. Gautieri, S. Vesentini, A. Redaelli and M. J. Buehler, *Nano Letters*, 2011, **11**, 757–766.

3 M. Sun, B. K. Connizzo, S. M. Adams, B. R. Freedman, R. J. Wenstrup, L. J. Soslowsky and D. E. Birk, *The American Journal of Pathology*, 2015, **185**, 1436–1447.

4 A. Hakim and R. Grahame, *Best Practice & Research Clinical Rheumatology*, 2003, **17**, 989–1004.

5 K. Wang and Z. Wang, *Journal of the Mechanics and Physics of Solids*, 2023, **178**, 105350.

6 L. Turner, W. S. Ryu and H. C. Berg, *Journal of Bacteriology*, 2000, **182**, 2793–2801.

7 H. Tuazon, E. Kaufman, D. I. Goldman and M. S. Bhamla, *Integrative and Comparative Biology*, 2022, **62**, 890–896.

8 M. Ashby, *Scripta Materialia*, 2013, **68**, 4–7.

9 Y. Estrin, Y. Beygelzimer, R. Kulagin, P. Gumbsch, P. Fratzl, Y. Zhu and H. Hahn, *Materials Research Letters*, 2021, **9**, 399–421.

10 S. G. Higgins, M. Becce, A. Belessiotis-Richards, H. Seong, J. E. Sero and M. M. Stevens, *Advanced Materials*, 2020, **32**, 1903862.

11 F. J. Harding, S. Surdo, B. Delalat, C. Cozzi, R. Elnathan, S. Gronthos, N. H. Voelcker and G. Barillaro, *ACS Appl. Mater. Interfaces*, 2016, **8**, 29197–29202.

12 R. Elnathan, B. Delalat, D. Brodoceanu, H. Alhmoud, F. J. Harding, K. Buehler, A. Nelson, L. Isa, T. Kraus and N. H. Voelcker, *Advanced Functional Materials*, 2015, **25**, 7215–7225.

13 N. Yanai and S. Granick, *Angewandte Chemie International Edition*, 2012, **51**, 5638–5641.

14 C. M. Stafford, K. E. Roskov, T. H. Epps and M. J. Fasolka, *Review of Scientific Instruments*, 2006, **77**, 023908.

15 H. S. Kim, C. H. Lee, P. K. Sudeep, T. Emrick and A. J. Crosby, *Advanced Materials*, 2010, **22**, 4600–4604.

16 S. Choudhary and A. J. Crosby, *Journal of Polymer Science Part B: Polymer Physics*, 2018, **56**, 1545–1551.

17 D. Y. Lee, J. T. Pham, J. Lawrence, C. H. Lee, C. Parkos, T. Emrick and A. J. Crosby, *Advanced Materials*, 2013, **25**, 1248–1253.

18 R. D. Deegan, O. Bakajin, T. F. Dupont, G. Huber, S. R. Nagel and T. A. Witten, *Nature*, 1997, **389**, 827–829.

19 J. T. Pham, J. Lawrence, D. Y. Lee, G. M. Grason, T. Emrick and A. J. Crosby, *Advanced Materials*, 2013, **25**, 6703–6708.

20 L. Prévost, D. M. Barber, M. Daïeff, J. T. Pham, A. J. Crosby, T. Emrick, O. du Roure and A. Lindner, *ACS Nano*, 2022, **16**, 10581–10588.

21 C. L. Bower, E. A. Simister, E. Bonnist, K. Paul, N. Pightling and T. D. Blake, *AIChE Journal*, 2007, **53**, 1644–1657.

22 S. Choudhary and A. J. Crosby, *Journal of Polymer Science, Part B: Polymer Physics*, 2019, **57**, 1270–1278.

23 G. Reiter, *Phys. Rev. Lett.*, 1992, **68**, 75–78.

24 G. Reiter, *Langmuir*, 1993, **9**, 1344–1351.

25 E. S. Petek and R. Katsumata, *Macromolecular Chemistry and Physics*, 2023, **224**, 2200375.

26 C. V. Thompson, *Annual Review of Materials Research*, 2012, **42**, 399–434.

27 L. Xue and Y. Han, *Progress in Polymer Science*, 2011, **36**, 269–293.

28 P. Müller-Buschbaum, J. S. Gutmann, C. Lorenz-Haas, O. Wunnicke, M. Stamm and W. Petry, *Macromolecules*, 2002, **35**, 2017–2023.

29 G. Reiter, *Macromolecules*, 1994, **27**, 3046–3052.

30 G. Reiter, A. Sharma, A. Casoli, M.-O. David, R. Khanna and P. Auroy, *Langmuir*, 1999, **15**, 2551–2558.

31 R. Xie, A. Karim, J. F. Douglas, C. C. Han and R. A. Weiss, *Phys. Rev. Lett.*, 1998, **81**, 1251–1254.

32 J. Brandrup and E. H. Immergut, Eds., *Polymer handbook*, Wiley, New York, 3rd ed., 1989.

33 L. M. Dossin and W. W. Graessley, *Macromolecules*, 1979, **12**, 123–130.

34 Y. -H. Hsu, J. E. Mark and B. Erman, *J Polym Sci B Polym Phys*, 1993, **31**, 481–486.

35 S. Xu, P. A. O'Connell and G. B. McKenna, *The Journal of Chemical Physics*, 2010, **132**, 184902.

36 X. Li and G. B. McKenna, *Macromolecules*, 2015, **48**, 6329–6336.